ARCHIVES OF ELECTRICAL ENGINEERING VOL. 73(4), pp. 927–939 (2024)

DOI 10.24425/aee.2024.152103

Infinite-time optimal feedback control of a 3-phase asynchronous motor exploiting a nonlinear finite element model

CEZARY JEDRYCZKA [1]✉, SŁAWOMIR STEPIEN [2], ANDRZEJ DEMENKO [1], MIROSŁAW NOWAKOWSKI [3]

[1] *Institute of Electrical Engineering and Electronics Poznan University of Technology Piotrowo 3a, 60-965 Poznan, Poland*

[2] *Institute of Automatic Control and Robotics, Poznan University of Technology Piotrowo 3a, 60-965 Poznan, Poland*

[3] *Air Force Institute of Technology Ksiecia Boleslawa St. 6, 01-494 Warsaw, Poland*

e-mail: {✉ cezary.jedryczka/slawomir.stepien/andrzej.demenko}@put.poznan.pl, miroslaw.nowakowski@itwl.pl

(Received: 06.01.2024, revised: 16.11.2024)

Abstract: This paper presents modelling of a squirrel-cage induction motor and an optimal control method based on suboptimal control for nonlinear systems to minimise consumed energy and power losses in an induction motor drive. A coupled motor model with optimal control as a closed-loop integrated system is proposed. For modelling of the squirrel-cage asynchronous machine, a field-circuit-mechanical finite-element (FE) model is employed, in which mechanical motion is realised by a moving-mesh method and fixed mesh approach. For the control problem purpose, a surrogate induction motor model, described in a stationary rotor reference d–q frame, is applied. The optimal control is realised by a nonlinear feedback compensator method based on the state-dependent Riccati equation (SDRE) with an infinite time horizon with the surrogate model state-dependent parametrisation (SDP). To perform the control strategy, a SDRE technique with Moore–Penrose pseudoinverse is adopted. To improve the accuracy of the optimisation procedure, a finite element model was used to calculate the motor performance.

Key words: finite element method, optimal control theory, state-dependent Riccati equation

1. Introduction

Accurate and precise control of electric motors is an area of active research worldwide. Research being carried out focusses on finding control methods for drive systems that ensure high robustness to external disturbances in terms of achieving specific trajectories while minimising

associated errors in position, speed or torque of the drive system [1–3]. The scope of literature in this area is vast, but some specific topics deserve attention, in particular optimal control theory [3–8], sliding control methods [2,3], adaptive control employing neural network techniques, fuzzy logic and genetic algorithms [9–11]. A common goal of the approaches discussed is to minimise energy losses in the motor windings, as well as energy supplied from the source itself. This can be achieved by determining the optimal switching angles of the phase excitation, as discussed, for example, in articles [12] and [13]. One of the most suitable approaches to optimal current control is the use of finite element (FE) modelling of the magnetic field to accurately determine the energy distribution, which allows the application of optimal control theory with a nonlinear state-dependent current controller [7,8]. The presented approach was published in an abbreviated form as part of a conference abstract [14], of which the current article is an extension that contains a detailed description of the control method and the motor modelling techniques. Thus, the paper presents a complete study related to modelling (including surrogate modelling) and control of induction motor drives. Thus, the main contribution in this paper is the conception and design of the control system, where the squirrel-cage motor is modelled by the FE approach and coupled to a closed-loop integrated system performing the optimal control strategy, employing the surrogate model of the induction machine and the SDRE technique.

2. FE and surrogate model of the squirrel-cage motor

The field circuit model of the asynchronous squirrel-cage machine has been employed. In the model two formulations have been applied. The formulation $\boldsymbol{A}$–V with vector magnetic potential $\boldsymbol{A}$ and scalar electric V has been used to describe the electromagnetic field in the rotor region with the squirrel-cage winding [15]. The stator region with stranded winding has been modelled using the $\boldsymbol{A}$–$\boldsymbol{T}_0$ method with electric vector potential $\boldsymbol{T}_0$ to represent winding current [15–17]. The edge values of potentials $\boldsymbol{A}$ and $\boldsymbol{T}_0$ have been applied. It should be noted that the edge values of $\boldsymbol{T}_0$ represent the loop currents in the stator windings and simplify linking the field equations with circuit equations of the supply and control system.

In the considered drive the field model can be simplified by assuming that the magnetic flux in the direction parallel to the rotor shaft is negligibly small. Due to this simplification, the stator end windings are represented by lumped parameters, i.e., resistances and inductances. Moreover, the 2.5D approach presented in [18] has been used to model the rotor slot skew.

The proposed field circuit model should be adapted to the analysis of motor drive transients. Therefore, it is important to formulate an appropriate method of rotor movement simulation and formulas of torque calculation. Two methods of rotor movement simulation have been analysed: (a) the moving-mesh method with the band of remeshing elements in the air gap and (b) less computationally-consuming, the fixed mesh method [18]. The moving-mesh method is more accurate and enables one to investigate the effects of the higher harmonics of the moving magnetic wave, e.g. to investigate the parasitic torques. However, in the analysis of the optimal control of the considered drive these effects do not need to be taken into account. Therefore, to reduce computation time, the fixed mesh method given in [5] has been applied. In this method, the time-stepping scheme is applied. The procedure of time derivative calculation is supported by a harmonic analysis of the potential distribution in the bars [15,18].

The efficient motor control requires a precise description of the electromagnetic torque acting on the rotor. In order to obtain the formula that describes electromagnetic torque the virtual work principle has been applied. The rotor region has been represented by a region with magnetisation and conduction currents. In the discrete FE model these currents are represented by the vector of magnetomotive forces associated with finite element edges. The torque has been expressed as a derivative of magnetic coenergy in terms of the virtual angular displacement of these magnetomotive forces. The FE representation of the virtual displacement is similar to the applied method of movement simulation. Thanks to that approach, the calculated torque is free of 'ripple' caused by non-compliance of the calculation procedure with the discrete FE model. As a result of FE method application the field equations are approximated by a system of nonlinear differential equations. Further on these equations for the stator region and the rotor will be presented separately. The FE model of the stator region consists of equations that describe magnetic field distribution and a circuit equation that defines the currents in stator windings. In the applied FE method, the magnetic field is expressed in terms of the edge values of magnetic vector potential $\boldsymbol{A}$ and the stator currents $\boldsymbol{i}$ are represented by the edge value of $\boldsymbol{T}_0$. These FE and circuit equations can be written in the following matrix form [18]:

$$\begin{bmatrix} \boldsymbol{S} & -\boldsymbol{z}^T \\ p\boldsymbol{z} & \boldsymbol{R}_w + p\boldsymbol{L}_w \end{bmatrix} \begin{bmatrix} \boldsymbol{\varphi} \\ \boldsymbol{i} \end{bmatrix} = \begin{bmatrix} 0 \\ \boldsymbol{u} \end{bmatrix}. \tag{1}$$

Here, $\boldsymbol{S}$ is the reluctance (stiffness) matrix, φ is the vector that consists of edge values of magnetic vector potential $\boldsymbol{A}$, $p = \mathrm{d}/\mathrm{d}t$, $\boldsymbol{R}_w$ is the diagonal matrix of winding resistances, $\boldsymbol{L}_w$ is the matrix of end-turn inductances, $\boldsymbol{u}$ and $\boldsymbol{i}$ are vectors of supply voltages and motor currents, respectively. Matrix $\boldsymbol{z}$ describes the winding distribution in the FE space and transforms the edge values of the magnetic vector potential into the flux linkages of the phase windings. The element of the u-th row and v-th column of $\boldsymbol{z}$ is equal to the number of conductors of phase u in the region associated with the v-th edge of the mesh. It should be noted that the edge values of $\boldsymbol{A}$ represent loop fluxes in the loops around the edges of the element. Thus, the expression $\boldsymbol{z}p\varphi$ describes electromotive force (emf) in the stator windings. For each phase winding, this emf is completed by emf caused by end-turn leakage flux, $\boldsymbol{L}_w\boldsymbol{i}$.

The applied model of a squirrel-cage winding includes the eddy current in the rotor bars. To represent the skew of rotor slots and bars, the rotor region is divided into segments of different positions in relation to the stator. It has been assumed that the current density in each bar segment has only a component parallel to the bar. Because of this assumption, the distribution of electric potential V can be easily determined analytically. For the i-th bar segment of length l_i we obtain $\mathrm{grad}V = u_{si}/l_i$, where u_{si} is the voltage across the bar segment. Consequently, the problem of solving the FE equations for potential V is replaced with the problem of solving the circuit equations describing voltages $\boldsymbol{u}_s$ across the bar segments and bar currents $\boldsymbol{i}_b$.

These equations and the equations describing the edge values of potential $\boldsymbol{A}$ can be written as follows:

$$\begin{bmatrix} \boldsymbol{S} + \boldsymbol{G}p & -\boldsymbol{z}^T \\ -\boldsymbol{k}_c\boldsymbol{G}p & (\boldsymbol{k}_c\boldsymbol{G}\boldsymbol{k}_c^T)^{-1} \end{bmatrix} \begin{bmatrix} \boldsymbol{\varphi} \\ \boldsymbol{u}_b \end{bmatrix} = \begin{bmatrix} 0 \\ \boldsymbol{i}_b \end{bmatrix}, \tag{2}$$

where $\boldsymbol{G}$ is the matrix of conductances associated with the edges of the mesh, and matrix $\boldsymbol{k}_c$ transforms the currents associated with the element edges into the total currents $\boldsymbol{i}_b$ in the bars.

The presented above equation for rotor segments should be completed by the equations that describe the segment connections and the connection of bars with end-rings. It was assumed that end-rings can be represented by equivalent, concentrated resistance R_e and inductance L_e of the end-ring segment. Here the end-ring segment is the part of the ring between the two neighbouring bars. In the considered motor, end-rings on both sides of the rotor are identical; therefore, in the circuit equations for the loops with bars and end-ring segments resistance R_e and inductance L_e are multiplied by 2:

$$\boldsymbol{i}_b = \boldsymbol{k}_e \boldsymbol{i}_e, \tag{3}$$

$$2(R_e + pL_e)\boldsymbol{i}_e + \boldsymbol{k}_e \boldsymbol{k}_s^T \boldsymbol{u}_s = 0. \tag{4}$$

Here: $\boldsymbol{i}_e$ is a vector of currents in the end-ring segments, the matrix $\boldsymbol{k}_s$ transforms the voltages $\boldsymbol{u}_s$ into the voltages $\boldsymbol{u}_b$ across the bars ($\boldsymbol{u}_b = \boldsymbol{k}_s \boldsymbol{u}_s$) and $\boldsymbol{k}_e$ is the connection matrix that transforms the currents in the end-ring segments into the currents in bars [15, 18]. The solution for a time-dependent field is obtained using the time-stepping method. The Crank–Nicolson schema is used. However, in order to avoid non-monotonicity, a fully implicit schema is applied at the beginning of the analysed time period.

In FE modelling there is a problem of modelling distributed parameters because the state depends not only on time but also on space configuration (plane configuration in this case). Obtaining an optimal control law for this model could be difficult and would require too much computational effort. Thus, based on the efficient modelling technique, a surrogate state-space model seems to be more suitable and smart to obtain the mentioned control law. The model should be both simple and useful.

The induction motor model is described by equations that are expressed in a stationary rotor reference d–q frame. The d-axis aligns with the a-axis. All quantities in the rotor reference frame are referred to the stator:

$$\frac{\mathrm{d}}{\mathrm{d}t}\begin{bmatrix}\Psi_{sd}\\ \Psi_{sq}\end{bmatrix} = \begin{bmatrix}v_{sd}\\ v_{sq}\end{bmatrix} - R_s\begin{bmatrix}i_{sd}\\ i_{sq}\end{bmatrix} - \omega_{da}\begin{bmatrix}0 & -1\\ 1 & 0\end{bmatrix}\begin{bmatrix}\Psi_{sd}\\ \Psi_{sq}\end{bmatrix}, \tag{5}$$

$$\frac{\mathrm{d}}{\mathrm{d}t}\begin{bmatrix}\Psi_{rd}\\ \Psi_{rq}\end{bmatrix} = \begin{bmatrix}v_{rd}\\ v_{rq}\end{bmatrix} - R_r\begin{bmatrix}i_{rd}\\ i_{rq}\end{bmatrix} - \omega_{dA}\begin{bmatrix}0 & -1\\ 1 & 0\end{bmatrix}\begin{bmatrix}\Psi_{rd}\\ \Psi_{rq}\end{bmatrix}, \tag{6}$$

where fluxes are functions of motor currents

$$\begin{bmatrix}\Psi_{sd}\\ \Psi_{sq}\\ \Psi_{rd}\\ \Psi_{rq}\end{bmatrix} = \begin{bmatrix}L_s & 0 & L_m & 0\\ 0 & L_s & 0 & L_m\\ L_m & 0 & L_r & 0\\ 0 & L_m & 0 & L_r\end{bmatrix}\begin{bmatrix}i_{sd}\\ i_{sq}\\ i_{rd}\\ i_{rq}\end{bmatrix}. \tag{7}$$

Ψ_{sd}, Ψ_{sq}, Ψ_{rd}, Ψ_{rq} are the stator and rotor q and d fluxes, i_{sd}, i_{sq}, i_{rd}, i_{rq} are the stator and rotor q and d currents, v_{sd}, v_{sq}, v_{rd}, v_{rq} are the stator and rotor q and d voltages, ω_{da} is the d–q stator electrical speed with respect to the rotor a-axis and ω_{dA} is the d–q stator electrical speed with respect to the rotor A-axis, R_s and R_r are the resistances of the stator and rotor winding, L_s, L_r, and L_m are the stator, rotor and magnetising inductance, respectively.

To calculate the d–q rotor electrical speed with respect to the rotor A-axis (dA), the model uses the difference between the stator a-axis (da) speed and slip speed:

$$\omega_{dA} = \omega_{da} - \omega_{dm}. \tag{8}$$

To simplify the equations for the flux, voltage, and current transformations, using a stationary reference frame, the speeds (8) are

$$\omega_{da} = 0 \quad \text{and} \quad \omega_{dA} = \omega_{em} = P\omega_m, \tag{9}$$

where ω_{em}, ω_m, P are the electrical rotor speed, angular velocity of the rotor and the number of pole pairs, respectively.

The full 3-phase asynchronous motor model must also include a motion equation.

$$J\frac{\mathrm{d}\omega_m}{\mathrm{d}t} + b\omega_m = T_e - T_{\text{load}}, \tag{10}$$

where T_{load} is the load torque and the electromagnetic motor torque T_e is the nonlinear function of motor currents.

$$T_e = PL_m(i_{sq}i_{rd} + i_{sd}i_{rq}), \tag{11}$$

where b and J are the damping and rotor inertia, respectively.

Neglecting T_{load} in (10), above Eqs. (5), (6) coupled with (10) can be written in one system of nonlinear equations in state-space form:

$$\begin{bmatrix} L_s & 0 & L_m & 0 & 0 \\ 0 & L_s & 0 & L_m & 0 \\ L_m & 0 & L_r & 0 & 0 \\ 0 & L_m & 0 & L_r & 0 \\ 0 & 0 & 0 & 0 & J \end{bmatrix} \begin{bmatrix} \frac{\mathrm{d}i_{sd}}{\mathrm{d}t} \\ \frac{\mathrm{d}i_{sq}}{\mathrm{d}t} \\ \frac{\mathrm{d}i_{rd}}{\mathrm{d}t} \\ \frac{\mathrm{d}i_{rq}}{\mathrm{d}t} \\ \frac{\mathrm{d}\omega_m}{\mathrm{d}t} \end{bmatrix} = \begin{bmatrix} R_s & 0 & 0 & 0 & 0 \\ 0 & R_s & 0 & 0 & 0 \\ 0 & -P\omega_m L_r & R_r & -P\omega_m L_r & 0 \\ P\omega_m L_m & 0 & P\omega_m L_r & R_r & 0 \\ PL_m i_{rq} & PL_m i_{rq} & 0 & 0 & -b \end{bmatrix} \begin{bmatrix} i_{sd} \\ i_{sq} \\ i_{rd} \\ i_{rq} \\ \omega_m \end{bmatrix} + \begin{bmatrix} 1 & 0 \\ 0 & 1 \\ 0 & 0 \\ 0 & 0 \\ 0 & 0 \end{bmatrix} \begin{bmatrix} v_{sd} \\ v_{sq} \end{bmatrix}, \tag{12}$$

or shortly writing

$$\boldsymbol{E}_{dq}\dot{\boldsymbol{x}}_{dq} = \boldsymbol{G}_{dq}(\boldsymbol{x}_{dq})\boldsymbol{x}_{dq} + \boldsymbol{H}\boldsymbol{u}_{dq}, \tag{13}$$

where

$$\boldsymbol{x}_{dq} = \begin{bmatrix} i_{sd} & i_{sq} & i_{rd} & i_{rq} & \omega_m \end{bmatrix}^T \tag{14}$$

and

$$\boldsymbol{u}_{dq} = \begin{bmatrix} v_{sd} & v_{sq} \end{bmatrix}^T. \tag{15}$$

The stator phase voltages and currents are computed by power invariant d–q transformation to ensure that the d–q and three-phase powers are equal:

$$\begin{bmatrix} v_{sd} \\ v_{sq} \end{bmatrix} = \sqrt{\frac{2}{3}} \begin{bmatrix} \cos(\theta_{da}) & \cos(\theta_{da} - k) & \cos(\theta_{da} + k) \\ \sin(\theta_{da}) & \sin(\theta_{da} - k) & \sin(\theta_{da} + k) \end{bmatrix} \begin{bmatrix} v_a \\ v_b \\ v_c \end{bmatrix} \tag{16}$$

and

$$\begin{bmatrix} i_{sd} \\ i_{sq} \end{bmatrix} = \sqrt{\frac{2}{3}} \begin{bmatrix} \cos(\theta_{da}) & \cos(\theta_{da} - k) & \cos(\theta_{da} + k) \\ \sin(\theta_{da}) & \sin(\theta_{da} - k) & \sin(\theta_{da} + k) \end{bmatrix} \begin{bmatrix} i_a \\ i_b \\ i_c \end{bmatrix}, \tag{17}$$

where $k = 2\pi/3$.

Considering the AC motor model described by (13) and the applied d–q transformation (16)–(17), for the control problem purpose, the motor model can be rewritten in a useful form:

$$\boldsymbol{E}\dot{\boldsymbol{x}} = \boldsymbol{G}(\boldsymbol{x})\boldsymbol{x} + \boldsymbol{H}\boldsymbol{u}, \tag{18}$$

where

$$\boldsymbol{x} = \begin{bmatrix} i_a & i_b & i_c & \omega_m \end{bmatrix}^T \tag{19}$$

and

$$\boldsymbol{u} = \begin{bmatrix} u_a & u_b & u_c \end{bmatrix}^T. \tag{20}$$

3. SDRE control formulation

Optimal control theory concentrates on optimising a control law that brings a dynamic system from a certain initial state to a certain final state, by requiring the control law to minimise the objective function associated with the system. In the case of minimizing energy in an ASM drive system, the linear-quadratic performance index is a reasonable solution [7]. It allows one to find optimal waveforms of the excitation voltage supplied to the motor windings in terms of minimising the supplied energy and power losses in the winding resistance. The control problem is to find the optimal control that minimises the following objective function

$$J(\boldsymbol{u}) = \frac{1}{2}\int_0^\infty (\boldsymbol{x}^T\boldsymbol{Q}\boldsymbol{x} + \boldsymbol{u}^T\boldsymbol{R}\boldsymbol{u})\,\mathrm{d}t, \tag{21}$$

where: $\boldsymbol{Q}$ is the symmetric, positive semi-definite weighting matrix for states, $\boldsymbol{R}$ is the symmetric, positive definite weighting matrix for control inputs, $\boldsymbol{u}$ is the vector of input voltages and $\boldsymbol{x}$ is the motor state vector.

Consider the nonlinear dynamic affine system

$$\dot{\boldsymbol{x}} = \boldsymbol{F}(\boldsymbol{x}) + \boldsymbol{B}\boldsymbol{u}. \tag{22}$$

In this case, the control problem formulation is stated as in classic SDRE form, (21) and (22), but the SDC parameterised form of (22) uses the separated form of matrix $\boldsymbol{C}(\boldsymbol{x})$:

$$\dot{\boldsymbol{x}} = \boldsymbol{C}(\boldsymbol{x})\boldsymbol{x} + \boldsymbol{B}\boldsymbol{u} = (\boldsymbol{C}_1 + \boldsymbol{C}_2(\boldsymbol{x}))\boldsymbol{x} + \boldsymbol{B}\boldsymbol{u}, \tag{23}$$

As in the previous case of checking the controllability of the affine system (23), the pair of components $\{\boldsymbol{C}_1, \boldsymbol{B}\}$ should be controllable. It means that the controllability matrix

$$\boldsymbol{M}(\boldsymbol{x}) = \begin{bmatrix} \boldsymbol{B} & \boldsymbol{C}_1\boldsymbol{B} & \dots & \boldsymbol{C}_1^{n-1}\boldsymbol{B} \end{bmatrix} \tag{24}$$

should have a full rank. Using Hamiltonian theory

$$H = \frac{1}{2}\Big(\boldsymbol{x}^T\boldsymbol{Q}\boldsymbol{x} + \boldsymbol{u}^T\boldsymbol{R}\boldsymbol{u} + \boldsymbol{p}^T((\boldsymbol{C}_1 + \boldsymbol{C}_2(\boldsymbol{x}))\boldsymbol{x} + \boldsymbol{B}\mathbf{u})\Big), \tag{25}$$

and considering the Pontryagin minimum principle, the necessary optimality condition $\partial H/\partial \boldsymbol{u} = 0$ with $\boldsymbol{p} = ((\boldsymbol{K}_1 + \boldsymbol{K}_2(\boldsymbol{x}))\boldsymbol{x}$, results in a control law as

$$\boldsymbol{u} = -\boldsymbol{R}^{-1}\boldsymbol{B}^T\left(\boldsymbol{K}_1 + \boldsymbol{K}_2\left(\boldsymbol{x}\right)\right)\boldsymbol{x}. \tag{26}$$

The control law in (26) includes two feedback compensators. The first is constant and the second is state-dependent. Employing the optimality condition and control law in (26), the nonlinear system is described by the state-space equation

$$\dot{x} = \left(\boldsymbol{C}_1 + \boldsymbol{C}_2\left(\boldsymbol{x}\right)\right)\boldsymbol{x} - \boldsymbol{B}\boldsymbol{R}^{-1}\boldsymbol{B}^T\boldsymbol{p}, \tag{27}$$

and adjoints the differential equation

$$\dot{\boldsymbol{p}} = -\left(\boldsymbol{C}_1 + \frac{\partial\left(\boldsymbol{C}_2\left(\boldsymbol{x}\right)\boldsymbol{x}\right)}{\partial \boldsymbol{x}}\right)^T\boldsymbol{p} - \boldsymbol{Q}\boldsymbol{x}, \tag{28}$$

where

$$\frac{\partial\left(\boldsymbol{C}_2\left(\boldsymbol{x}\right)\boldsymbol{x}\right)}{\partial \boldsymbol{x}} = \boldsymbol{C}_2\left(\boldsymbol{x}\right) + \frac{\partial \boldsymbol{C}_2\left(\boldsymbol{x}\right)}{\partial \boldsymbol{x}}\boldsymbol{x}. \tag{29}$$

Substituting $\boldsymbol{p} = (\boldsymbol{K}_1 + \boldsymbol{K}_2(\boldsymbol{x}))\boldsymbol{x}$ into (27) the closed-loop state-space nonlinear equation can be written as

$$\dot{\boldsymbol{x}} = \left(\boldsymbol{C}_1 - \boldsymbol{B}\boldsymbol{R}^{-1}\boldsymbol{B}^T\boldsymbol{K}_1\right)\boldsymbol{x} + \left(\boldsymbol{C}_2\left(\boldsymbol{x}\right) - \boldsymbol{B}\boldsymbol{R}^{-1}\boldsymbol{B}^T\boldsymbol{K}_2\left(\boldsymbol{x}\right)\right)\boldsymbol{x}. \tag{30}$$

The first bracket of Eq. (14) is state-independent, the second one is state-dependent, thus there is a possibility to linearise it and solve the state-dependent gain matrix $\boldsymbol{K}_2(\boldsymbol{x})$

$$\boldsymbol{K}_2\left(\boldsymbol{x}\right) = \left[\boldsymbol{B}\boldsymbol{R}^{-1}\boldsymbol{B}^T\right]^{\dagger}\boldsymbol{C}_2\left(\boldsymbol{x}\right), \tag{31}$$

employing the Moore–Penrose pseudoinverse [19]. Then closed-loop system (14) takes the form

$$\dot{\boldsymbol{x}} = \left(\boldsymbol{C}_1 - \boldsymbol{B}\boldsymbol{R}^{-1}\boldsymbol{B}^T\boldsymbol{K}_1\right)\boldsymbol{x}, \tag{32}$$

because

$$\lim_{\|\boldsymbol{x}\|\to 0}\frac{\left\|\boldsymbol{C}_2\left(\boldsymbol{x}\right) - \boldsymbol{B}\boldsymbol{R}^{-1}\boldsymbol{B}^T\boldsymbol{K}_2\left(\boldsymbol{x}\right)\right\|\|\boldsymbol{x}\|}{\|\boldsymbol{x}\|} = 0. \tag{33}$$

From the above it can be seen that the compensator gain $\boldsymbol{K}(\boldsymbol{x}) = \boldsymbol{K}_1 + \boldsymbol{K}_2(\boldsymbol{x})$ can be obtained from (31) for $\boldsymbol{K}_2(\boldsymbol{x})$ and from the algebraic Riccati equation ARE for $\boldsymbol{K}_1$

$$\boldsymbol{C}_1^T\boldsymbol{K}_1 + \boldsymbol{K}_1\boldsymbol{C}_1 - \boldsymbol{K}_1\boldsymbol{B}\boldsymbol{R}^{-1}\boldsymbol{B}^T\boldsymbol{K}_1 + \boldsymbol{Q} = 0. \tag{34}$$

The control schema for the induction motor, including a surrogate state simulator and feedback compensator, is shown in Fig. 1.

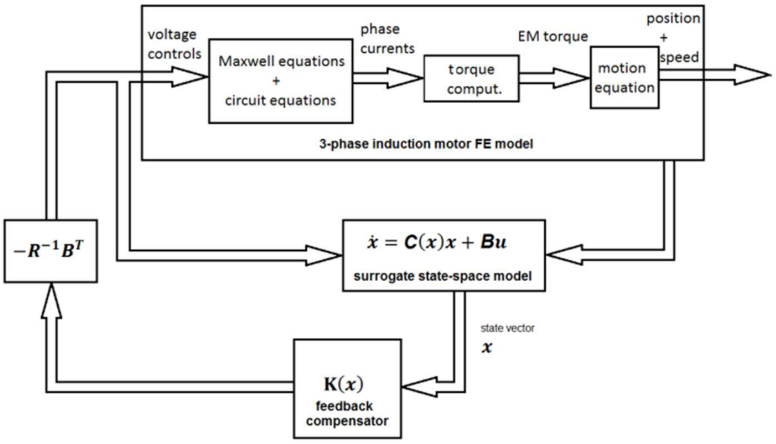

Fig. 1. Schema of an optimal control system

It is worthy to note that Eq. (34) is time-independent and needs to be solved only once in the control process. The same situation applies to operation (31). So, in comparison to the classic SDRE approach [7], the computational effort is strongly reduced. Then the implementation of the control law becomes much easier in a real control system.

4. Numerical experiments

The numerical model of the considered squirrel-cage asynchronous motor has been based on a general-purpose 3 kW, 4-pole asynchronous motor (ASM) of type SGL-100-4b. Due to the symmetry of the magnetic circuit, the geometry has been reduced – see the cross-section of the electromagnetic active part shown in Fig. 2.

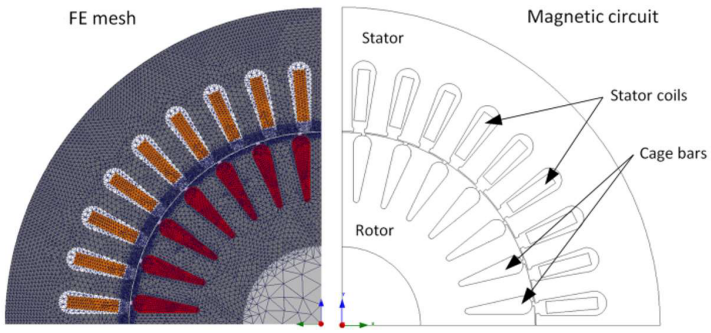

(a) (b)

Fig. 2. Applied FE mesh (a); magnetic circuit cross section (b)

The discretised model of a slice of the motor is presented in Fig. 2(a). Its discretisation grid has about 20 700 triangular elements. The time discretisation was set parametrically according to the controlled supply frequency by assuming the constant number of time steps for the period of supply voltage n_T is equal to 180. To examine the proposed control strategy, the phase voltages have been determined for three values of the reference frequency f_s equal to 10, 25 and 50 Hz, respectively. The optimal problem control is realised for finding motor state dynamics and SDRE control for the mentioned frequencies. In association with motor surrogate dynamics, the quadratic cost functional weighting matrices in (15) are chosen as

$$\boldsymbol{Q} = \begin{bmatrix} R & 0 & 0 & 0 & 0 \\ 0 & R & 0 & 0 & 0 \\ 0 & 0 & R & 0 & 0 \\ 0 & 0 & 0 & R & 0 \\ 0 & 0 & 0 & 0 & b \end{bmatrix}, \qquad \boldsymbol{R} = \begin{bmatrix} 1/R & 0 & 0 \\ 0 & 1/R & 0 \\ 0 & 0 & 1/R \end{bmatrix}. \tag{35}$$

Firstly, the optimal control is obtained by employing a surrogate motor model and next, the obtained control signals are applied to the FEM model. The determined phase voltage waveforms have been described by means of the amplitude coefficient and sine functions. The calculated amplitude coefficients for the examined reference frequencies are shown in Fig. 3(a) to Fig. 3(c).

Computed control signals for the considered frequencies give a linear relationship between frequency and voltage amplitude in a steady state. Very interesting is also the fact that the peak voltage generated at motor starting is also linear. It proves that the designed optimal controller works perfectly. The rotor speed and motor torque waveforms are shown in Fig. 4(a) and Fig. 4(b), respectively.

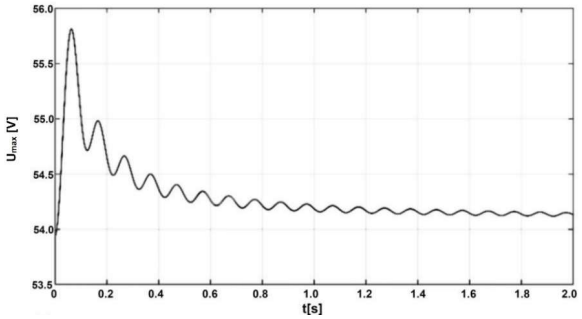

(a)

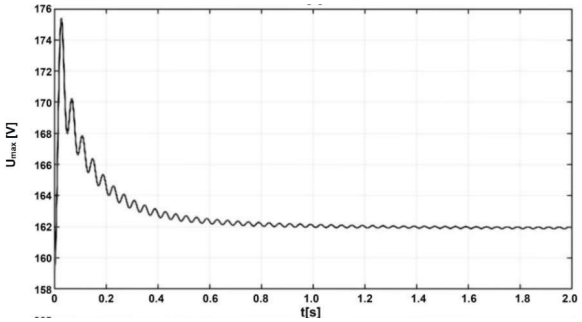

(b)

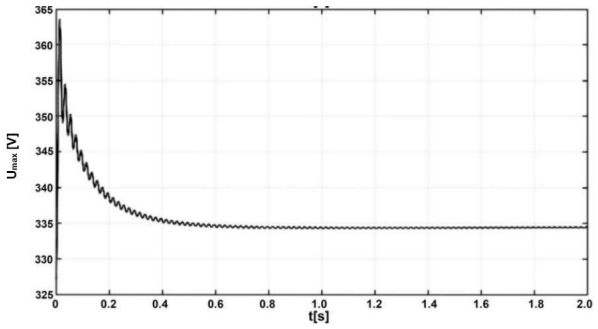

(c)

Fig. 3. Calculated amplitude coefficients of the motor phase voltages for f_s, equal to (a) 10 Hz; (b) 25 Hz and (c) 50 Hz

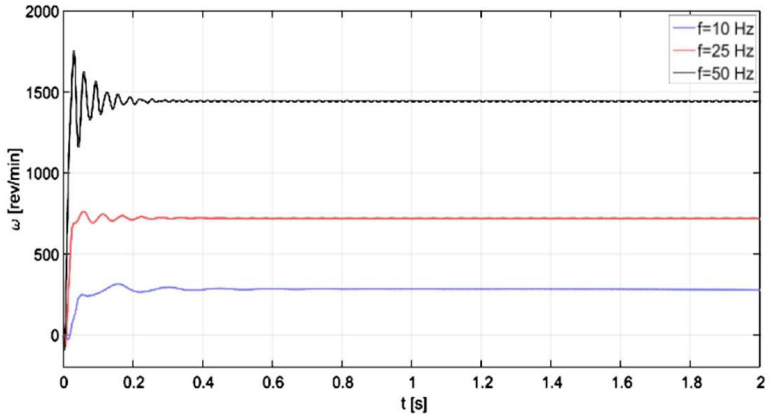

(a)

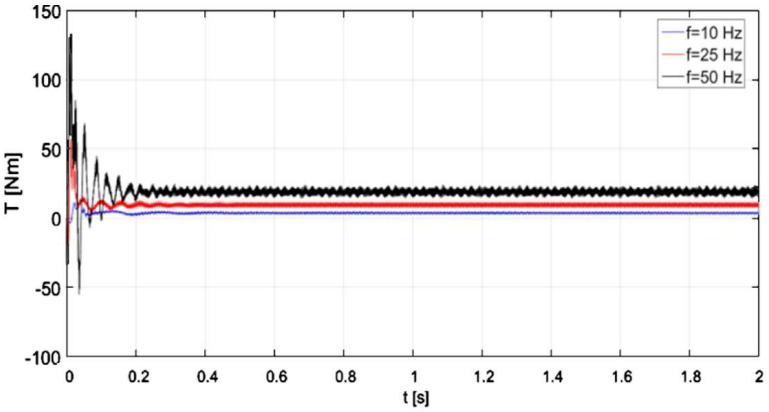

(b)

Fig. 4. Calculated speed (a) and torque (b) waveforms

As shown in Fig. 4(a), the relationship between the considered frequencies and obtained motor speeds is also linear, as expected. Frequency 50 Hz runs the motor on its nominal speed level, i.e. 1445 rpm with a small slip of 55 rpm. Lower frequencies enable controlling speed linearly. The analysis of torque waveforms presented in Fig. 4(b) gives the same remarks. The torque amplitude in a steady state can also be successively controlled by frequency in a linear way. The obtained phase currents from the FEM model of the motor are presented in Fig. 5. Their optimal amplitudes minimise the objective function value, (15), and are free of possible overshoots.

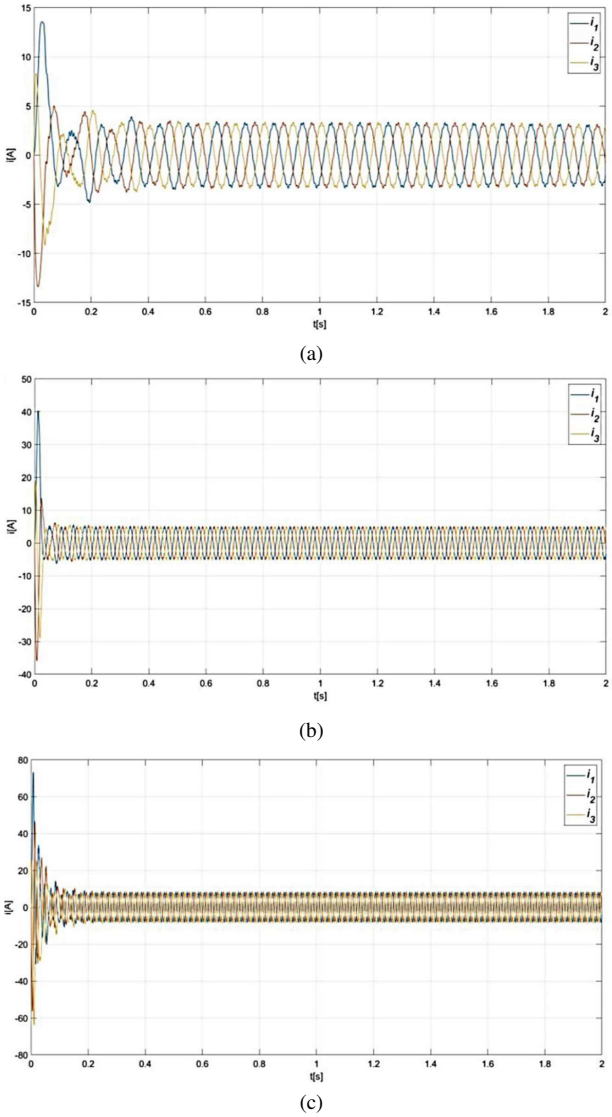

(a)

(b)

(c)

Fig. 5. Phase current waveforms calculated by means of the FEM model for f_s equal to (a) 10 Hz, (b) 25 Hz and (c) 50 Hz

5. Conclusions

The paper deals with numerical studies related to the optimal control of a 3-phase induction motor. Since the best approach to define optimal speed and current control is to use the finite element method (FEM) in magnetic field modelling to accurately determine energy distribution, optimal control theory with a nonlinear state-dependent current controller was used, in which the integral of the performance index includes energy supplied to the system and energy lost internally. The designed AC motor control system allows optimal control of speed, torque or phase currents with a linear dependence of the applied frequency. This makes control systems user-friendly and convenient. What is more, the optimisation function saves or minimizes energy expenses, also minimising control overshoot.

References

[1] Aghili F., *Adaptive reshaping of excitation currents for accurate torque control of brushless motors*, in IEEE Transactions on Control Systems Technology, vol. 16, no. 2, pp. 356–364 (2008), DOI: 10.1109/TCST.2007.908213.

[2] Brock S., *Sliding mode control of a permanent magnet direct drive under non-linear friction*, COMPEL - The international journal for computation and mathematics in electrical and electronic engineering, vol. 30, no. 3, pp. 853–863 (2011), DOI: 10.1108/03321641111110825.

[3] Allihalli H., Bayindir M.I., *Time-energy optimal control of vector controlled induction motor*, COMPEL - The international journal for computation and mathematics in electrical and electronic engineering, vol. 21, no. 2, pp. 235–251 (2002), DOI: 10.1108/03321640210416331.

[4] Bernat J., Stępień S., *Minimum energy control analysis of the switched reluctance stepper motor considering a nonlinear finite element model*, Simulation Modelling Practice and Theory, vol. 28, pp. 1–11 (2012), DOI: 10.1016/j.simpat.2012.05.005.

[5] Bernat J., Stępień S., *Modeling and optimal control of variable reluctance stepper motor*, COMPEL - The international journal for computation and mathematics in electrical and electronic engineering, vol. 30, no. 2, pp. 726–740 (2011), DOI: 10.1108/03321641111101177.

[6] Ignaciuk P., Bartoszewicz A., *Linear-quadratic optimal control of periodic-review perishable inventory systems*, in IEEE Transactions on Control Systems Technology, vol. 20, no. 5, pp. 1400–1407 (2012), DOI: 10.1109/TCST.2011.2161086.

[7] Banks H.T., Lewis B.M., Tran H.T., *Nonlinear feedback controllers and compensators: a state-dependent Riccati equation approach*, Computational Optimization and Applications, vol. 37, no. 2, pp. 177–218 (2007), DOI: 10.1007/s10589-007-9015-2.

[8] Çimen T., *Systematic and effective design of nonlinear feedback controllers via the state-dependent Riccati equation (SDRE) method*, Annual Reviews in Control, vol. 34, no. 1, pp. 32–51 (2010), DOI: 10.1016/j.arcontrol.2010.03.001.

[9] Mir S., Islam M.S., Sebastian T., Husain I., *Fault-tolerant switched reluctance motor drive using adaptive fuzzy logic controller*, in IEEE Transactions on Power Electronics, vol. 19, no. 2, pp. 289–295 (2004), DOI: 10.1109/TPEL.2003.823244.

[10] Cheng Z., Takahashi N., Forghani B., Gilbert G., Du Y., Fan Y., Liu L., Zhai Z., Wu W., Zhang J., *Effect of Excitation Patterns on Both Iron Loss and Flux in Solid and Laminated Steel Configurations*, in IEEE Transactions on Magnetics, vol. 46, no. 8, pp. 3185–3188 (2010), DOI: 10.1109/TMAG.2010.2044765.

[11] Jang G.H., Lee C.J., *Design and control of the phase current of a brushless dc motor to eliminate cogging torque*, Journal of Applied Physics, vol. 99, no. 8, 08R305 (2006), DOI: 10.1063/1.2165603.

[12] Bernat J., Kolota J., Stępień S., Sykulski J., *A steady state solver for modelling rotating electromechanical devices exploiting the transformation from time to position domain*, International Journal of Numerical Modelling: Electronic Networks, Devices and Fields, vol. 27, no. 2, pp. 213–228 (2014), DOI: 10.1002/jnm.1916.

[13] Mao S.H., Tsai M.C., *An analysis of the optimum operating point for a switched reluctance motor*, Journal of Magnetism and Magnetic Materials, vol. 282, pp. 53–56 (2004), DOI: 10.1016/j.jmmm.2004.04.012.

[14] Stepień S., Jedryczka C., Demenko A., *Optimal control of 3-phase induction machine exploiting a FEM model*, Tenth International Conference on Computational Electromagnetics (CEM 2019), Edinburgh, UK, pp. 1–2 (2019), DOI: 10.1049/cp.2019.0111.

[15] Jędryczka C., Wojciechowski R.M., Demenko A., *Finite element analysis of the asynchronous torque in LSPMSM with non-symmetrical squirrel cage winding*, International Journal of Applied Electromagnetics and Mechanics, vol. 46, no. 2, pp. 367–373 (2014), DOI: 10.3233/JAE-141947.

[16] Wojciechowski R.M., Demenko A., Sykulski J.K., *Comparative analysis of A-V and A-T-T0 calculations of induced currents in multiply connected regions*, IET Science Measurement & Technology, vol. 6, no. 5, pp. 312–318 (2012), DOI: 10.1049/iet-smt.2011.0114.

[17] Wojciechowski R.M., Jędryczka C., *A description of the sources of magnetic field using edge values of the current vector potential*, Archives of Electrical Engineering, vol. 67, no. 1 (2018), DOI: 10.24425/118988.

[18] Demenko A., Nowak L., *Finite element analysis of saturation effects in a squirrel cage electrical machine*, COMPEL - The international journal for computation and mathematics in electrical and electronic engineering, vol. 15, no. 4, pp. 88–95 (1996), DOI: 10.1108/03321649610154249.

[19] Barata J.C.A., Hussein M.S., *The Moore–Penrose Pseudoinverse. A Tutorial Review of the Theory*, Brazilian Journal of Physics, vol. 42, no. 1, pp. 146–165 (2012), DOI: 10.1007/s13538-011-0052-z.